X-ray natural birefringence in reflection from graphite

H.-Ch. Mertins,[1,*] P. M. Oppeneer,[2,3] S. Valencia,[4] W. Gudat,[4] F. Senf,[4] and P. R. Bressler[4]
[1]*University of Applied Sciences Münster, Stegerwaldstr. 39, D-48565 Steinfurt, Germany*
[2]*Leibniz-Institute of Solid State and Materials Research, P.O. Box 270016, D-01171 Dresden, Germany*
[3]*Department of Physics, Uppsala University, Box 530, S-751 21 Uppsala, Sweden*
[4]*BESSY GmbH, Albert-Einstein-Str. 15, D-12489 Berlin, Germany*
(Received 23 December 2003; published 3 December 2004)

The existence of the x-ray natural birefringence in reflection from graphite is demonstrated. This novel x-ray effect is measured as the polarization-plane rotation and ellipticity appearing upon reflection of linearly polarized synchrotron radiation from highly-oriented pyrolytic graphite. Polarization analysis is employed to measure the x-ray rotation and ellipticity spectra across the carbon 1*s* edge. Extraordinarily large birefringence rotation values of up to ±90 degrees as well as ellipticity values up to 30 degrees are detected across the carbon 1*s* absorption edge. To analyze the origin of the measured spectra, the Stokes parameters as well as the x-ray natural linear dichroism in reflection and absorption are determined across the C 1*s* edge. The strong birefringence near the C 1*s* absorption edge is shown to result directly from the optical anisotropy of hexagonal graphite. Measurements carried out on isotropic amorphous carbon films show in contrast a negligible birefringence. With its large birefringence and its reduced heat load sensitivity graphite bears potential as a tunable x-ray phase shifting $\lambda/4$ or $\lambda/2$ plate for future applications on new, high-intensity light sources.

DOI: 10.1103/PhysRevB.70.235106 PACS number(s): 78.20.Fm, 78.70.Ck, 78.70.Dm

I. INTRODUCTION

Natural optical effects in the x-ray regime are becoming increasingly popular. In contrast to the lively investigated x-ray magneto-optical effects, which require a time-reversal symmetry breaking due to a local exchange field, natural optical effects are present without such a symmetry-breaking field. However, some sort of internal symmetry breaking is required to bring about the natural optical effect. An overview of the rich variety of natural optical phenomena in the visible light range can be found in Refs. 1–3. Natural optical activity was discovered several years ago to exist as well in the x-ray regime for a chiral organometallic compound.[4] Other natural x-ray effects, as the x-ray natural circular dichroism[5] and the x-ray non-reciprocal linear gyrotropy were recently reported.[6] The origin of some of these effects is not well understood and is still being discussed.[7,8]

In contrast to spectroscopy with visible light, x-ray spectroscopy allows for element selective investigations by excitation of the individual atomic absorption levels. Most of the recent investigations of natural x-ray optical effects measured these in absorption, employing a yield technique.[4,5] An alternative way to investigate optical effects is polarization spectroscopy or ellipsometry, in which the full polarization state of the radiation after its interaction with the material is determined. In the x-ray regime polarization spectroscopy has gained increasing significance. It is a dedicated technique, with which, e.g., the complete set of Stokes parameters can be measured. When applied to the complex optical constants both their real and imaginary parts can directly be determined since both the phase and amplitude of the light after its interaction with matter is obtained. This relatively new x-ray ellipsometric method enabled recently the observations of the x-ray magneto-optical Faraday effect,[9,10] Kerr effect,[11] and Voigt effect.[12] These magneto-optical effects are now being more and more applied in the investigation of magnetic sensors and storage devices.

Here we report the observation of another novel phenomenon in the x-ray range, namely the x-ray natural birefringence of graphite detected in reflection. This effect can be regarded as the nonmagnetic analog of the x-ray Voigt effect.[12] The latter effect, however, is measured in transmission. To the best of our knowledge, the equivalent of the here reported optical effect has not been observed in the visible energy range. Optical anisotropy has, of course, been intensively studied in the visible range, where it can be detected by reflectivity or ellipsometric measurements performed sequentially along the nonequivalent optical axes (see, e.g., Ref. 13). In contrast, in the reflection geometry to be specified below, the x-ray birefringence in reflection is obtained in a single x-ray scattering measurement. In addition, as is the case for the Voigt effect too, the natural x-ray birefringence is observed as the plane rotation of linearly polarized light reflected from a uniaxial material having the optical axis oriented perpendicular to the surface. Also, the polarization state of the reflected light becomes elliptically polarized. In its appearance this x-ray optical effect does at first sight seem to be distinct from the usual optical birefringence, but, as will become evident below, it does in fact originate from the same source, namely, the optical constants being different for nonequivalent crystallographic axes. Using polarization analysis of the reflected light and incident linearly polarized synchrotron radiation we prove the existence of this effect with x-ray rotation and ellipticity spectra measured across the C 1*s* edge of highly-oriented pyrolytic graphite (HOPG). Our proposition, the observation of the x-ray natural birefringence, is compellingly underpinned by supplementary measurements of the Stokes parameters and the x-ray natural dichroism, for which analytical expressions relating these spectra to the birefringent polarization spectra can be derived. A comparison of the independently measured spectra supports the derived relationships. Furthermore, we present for comparison the corresponding spectra for amorphous car-

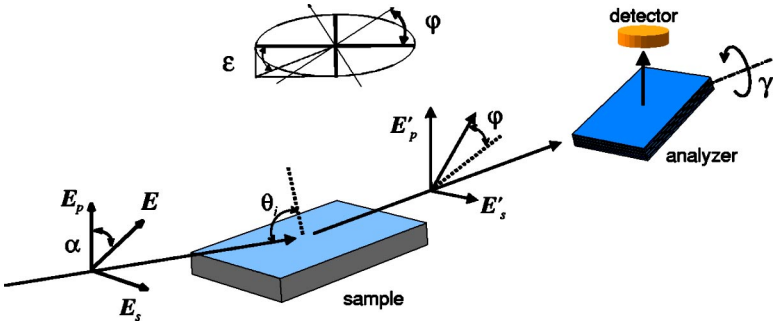

FIG. 1. (Color online) Experimental set-up for measuring the x-ray birefringence in reflection. Linearly polarized x-ray radiation is at glancing incidence to the film. The polarization plane and scattering plane are at an angle $\alpha=45°$. Upon reflection, the polarization plane of the reflected light is tilted over a rotation angle φ with respect to the incoming light. The reflected light has in addition become elliptically polarized. The polarization analysis is performed by rotating the analyzer mirror about γ.

bon, which exhibit a negligible birefringent effect. From the data for graphite we deduce directly the complete crystalline anisotropy in the optical constant, i.e., both real and imaginary parts.

It is important to note that the existence of the x-ray natural birefringence of graphite was predicted theoretically by Machavariani[14] a few years ago. Machavariani, being guided by the observation of anisotropies in the x-ray reflection from hexagonal BN crystals,[15] predicted the shape of some spectra for graphite. We compare our results to the predicted spectra, however, the agreement is not found to be overwhelmingly good. Nevertheless, we do observe a very large rotation, as was anticipated theoretically.

Apart from the spectroscopic interest, graphite has received considerable attention recently for other reasons. Graphite or related graphene layer materials are considered to be promising candidates for applications in future spin-electronic devices. The possible existence of ferromagnetism in graphite has been investigated both theoretically[16–18] and experimentally.[19,20] The first observations of weak ferromagnetism of graphite have been reported.[19–21] Also, graphite as well as C_{60} can be electron doped by alkali metals to become superconducting.[22] Most of the technologically relevant carbon based systems derive their properties of interest from the underlying graphite character. To study the electronic, magnetic, and structural properties of carbon or any other material, experiments with polarized synchrotron radiation are superbly suited. The important electronic states can be probed element selectively by tuning the excitation energy to the individual absorption edges of the atomic constituents (for example, the carbon 1*s* edge near 285 eV). Thus, by exploiting the polarization dependent interaction of light with matter electronic,[23,24] structural,[25] and magnetic information[26,27] can be obtained.

In the following we first outline the experimental set-up and derive theoretical expressions for the x-ray birefringence in reflection. In Sec. III our measured spectra are presented and discussed. Relationships between the x-ray natural dichroism and the x-ray birefringence are employed to discuss the origin of the measured spectra. Conclusions are given in Sec. IV.

II. THEORETICAL AND EXPERIMENTAL DESCRIPTION

A. Theory

We have employed the geometry shown schematically in Fig. 1 to detect the x-ray birefringence in reflection. The incident light is at a grazing angle to the surface and, in the most general configuration, linearly polarized at an angle α with respect to the refraction plane. For a nonzero value of $\alpha(\alpha<\pi/2)$ the light is in a mixed state of *s*-, and *p*-polarized light, similarly to the standard Voigt geometry for magnetic samples, where $\alpha=\pi/4$ gives the largest magneto-optical effect.[12] Upon reflection, the polarization plane is rotated by an angle φ, and, in addition, the light's polarization changes to ellipticaly polarized by an amount ε. In the following we consider the case $\alpha=\pi/4$, which leads to the largest birefringence effects. For $\alpha=\pi/4$ the incident light can be decomposed in two equal components: an *s* component parallel to the surface and an *p*-polarized component which at grazing incidence is nearly perpendicular to the surface. In our set-up the graphite layers lie in the surface plane, so that the optical axis of graphite is normal to the surface. The permittivity tensor of graphite contains—on account of the hexagonal crystal symmetry—only two nonequal diagonal elements, which we denote by $\varepsilon_\perp$ and $\varepsilon_\parallel$ for the direction normal and parallel, respectively, to the optical axis of the graphite film. While the nonequal permittivity components are expected to lead to birefringence, it is important to note that even in the case of an optically isotropic material the reflection of the E_s and E_p components can be anisotropic. This happens simply because the reflection coefficients $r_s(r_s=E_s'/E_s^0)$ and $r_p(r_p=E_p'/E_p^0)$ are unequal even for isotropic materials (see, e.g., Ref. 28). However, as we show below, in the particular case of grazing incidence in the soft-x-ray regime, the polarization rotation and ellipticity are a direct measure of the x-ray natural birefringence, i.e., these quantities arise because $\varepsilon_\perp$ and $\varepsilon_\parallel$ are nonequal.

To derive expressions for the polarization-plane rotation and ellipticity we apply the Fresnel formalism for crystal optics. The reflection coefficients r_p and r_s of the birefringent material are given by (see, e.g., Ref. 29)

$$r_p=\frac{\sqrt{\varepsilon_\parallel\varepsilon_\perp}\cos\theta_i-n_0\sqrt{\varepsilon_\parallel-n_0^2\sin^2\theta_i}}{\sqrt{\varepsilon_\parallel\varepsilon_\perp}\cos\theta_i+n_0\sqrt{\varepsilon_\parallel-n_0^2\sin^2\theta_i}}, \tag{1a}$$

$$r_s=\frac{n_0\cos\theta_i-\sqrt{\varepsilon_\perp-n_0^2\sin^2\theta_i}}{n_0\cos\theta_i+\sqrt{\varepsilon_\perp-n_0^2\sin^2\theta_i}}, \tag{1b}$$

where θ_i is the angle of incidence measured from the surface normal and n_0 is the optical constant of the initial dielectric medium. In the present configuration, the ordinary mode in the material stems from the initial *s*-polarized wave, while for $\theta_i>0$ the extraordinary mode stems from the initial

p-polarized wave. The rotation of the polarization plane and the ellipticity can be expressed in terms of r_s and r_p using the conventional Stokes formalism (see, e.g., Ref. 30), which gives

$$\frac{r_s - r_p}{r_s + r_p} = \frac{\tan\varphi + i\tan\varepsilon}{1 - i\tan\varphi\tan\varepsilon}. \tag{2}$$

Note that φ is defined here with respect to the polarization plane of the incoming light. From this equation exact expressions for $\varphi(\tan 2\varphi = (|r_s|^2 - |r_p|^2)/2\,\mathrm{Re}\{r_s r_p^*\})$ and ε $(\sin 2\varepsilon = 2\,\mathrm{Im}\{r_s r_p^*\}/(|r_s|^2 + |r_p|^2))$ can be derived. From these we obtain for φ and ε, to first order in the small quantity $\Delta \equiv \varepsilon_\parallel - \varepsilon_\perp$,

$$\tan 2\varphi + i\sin 2\varepsilon \approx 2\frac{r_s - r_p}{r_s + r_p} \approx \frac{2n_\perp \cos\theta_i \cos\theta_t}{n_0 \sin^2\theta_i} + \frac{n_0 \Delta \cos\theta_i}{n_\perp (n_0^2 - n_\perp^2)\sin^2\theta_i \cos\theta_t}, \tag{3}$$

where θ_t is the angle of refraction of the ordinary beam. At grazing incidence we can furthermore make an expansion with respect to the small angle $\vartheta = \pi/2 - \theta_i$, which leads to

$$\tan 2\varphi + i\sin 2\varepsilon \approx 2(n_\perp^2 - n_0^2)^{1/2}\frac{\sin\vartheta}{n_0} + \frac{n_0 \Delta \sin\vartheta}{(n_0^2 - n_\perp^2)^{3/2}}. \tag{4}$$

The first term is not related to any optical anisotropy, it would exist also for an isotropic material. In the soft-x-ray regime both $n_\perp$ and n_0 are close to 1, therefore it can be estimated that the second term is much larger (of the order of 1000Δ times) than the first term in the soft-x-ray regime. Consequently, we can neglect the first term for x-ray reflection from optically anisotropic crystals and approximate, for the vacuum/material interface, $\tan 2\varphi + i\sin 2\varepsilon \approx [(\varepsilon_\parallel - \varepsilon_\perp)/(1-n^2)^{3/2}]\sin\vartheta$, with $n \equiv 1/2(n_\parallel + n_\perp)$. Thus, in the soft x-ray regime the response in the reflected radiation is proportional to $(\varepsilon_\parallel - \varepsilon_\perp)$ which is the birefringence, i.e., $n_\parallel - n_\perp \approx (\varepsilon_\parallel - \varepsilon_\perp)/2n$. In the visible range, however, the second term of Eq. (4) is in contrast much smaller than the first term. We expect its smallness to be the reason that so far the natural birefringence in reflection has—to the best of our knowledge—not been detected utilizing this geometry in the visible range.

We can furthermore relate φ and ε to the conventional Stokes parameters S_1, S_2, and S_3 by

$$\tan 2\varphi = \frac{S_1}{S_2}, \quad \sin 2\varepsilon = S_3, \tag{5}$$

where the above given exact expressions for $\tan 2\varphi$ and $\sin 2\varepsilon$ were used. The Stokes parameters S_1, S_2, and S_3, which are normalized to the total intensity S_0 are determined through polarization analysis of the light reflected from the sample. The parameters S_1 and S_2 are the degrees of linear polarization in the *x*-*k* plane and in the plane diagonal to the *x*-*k* and *y*-*k* planes, respectively, with *k* the wave vector of the light. S_3 represents the degree of circular polarization. Our experimental set-up is chosen such that for the incident light $S_2 = 1$ and $S_1 = S_3 = 0$.

Although the reflection coefficients of *s*- and *p*-polarized light are not equal, we show that the x-ray birefringence can be detectable as well through intensity measurements of the reflectivities $R_s(=|r_s|^2)$ and $R_p(=|r_p|^2)$ at grazing incidence. To this end we define an asymmetry parameter $A \equiv (R_s - R_p)/(R_s + R_p)$, which can be directly related to the Stokes parameter S_1, or, alternatively, to φ through

$$A = S_1, \text{ and } A \approx \tan 2\varphi \approx 2\varphi. \tag{6}$$

The first expression is valid for all incident angles, whereas the second expression is only valid at grazing incidence and for small asymmetries and φ. At grazing incidence the asymmetry A is thus proportional to $\varepsilon_\parallel - \varepsilon_\perp$ and therefore this quantity is then precisely the x-ray natural linear dichroism (XNLD) in reflection. An identical relation was previously shown to exist between the x-ray magnetic linear dichroism (XMLD) and the x-ray magneto-optical Voigt effect,[12] which are both measured in transmission. The birefringent rotation of the polarization plane can thus be regarded as the "natural" analog of the Voigt rotation which is due to the magnetization induced difference between $\varepsilon_\parallel$ and $\varepsilon_\perp$. Note, that although both the XNLD parameter A and the Stokes parameter S_1 of the light after the interaction with the sample are thus correlated, they are measured independently by entirely different techniques. The XNLD can also be measured in absorption, in which case it would be proportional to $\mu_\parallel - \mu_\perp$, the difference of the respective absorption coefficients. Rewriting $\mu_\parallel - \mu_\perp$, shows that the XNLD in absorption is proportional to $\mathrm{Im}(\varepsilon_\parallel - \varepsilon_\perp)$.

B. Experimental aspects

The room-temperature experiments, schematically shown in Fig. 1, were performed on the undulator beamline UE52-SGM of BESSY.[31] The spectral resolution near 280 eV was $E/\Delta E = 2000$ and the accuracy of the energy calibration was better than 0.1 eV. The degree of linear polarization was $P_L > 0.99$. The angle of the electric field vector E of the linearly polarized incoming light was set to $\alpha = \pi/4$ with respect to the scattering plane, while the angle of incidence measured to the surface normal was set to $\theta_i = 87.5°$. To perform the polarization analysis of the reflected beam, we used the BESSY ultrahigh-vacuum polarimeter chamber.[32] The polarization of the incident or reflected beam was analyzed by rotating a W/C reflection multilayer (25 periods, of 3.09 nm each, angle of incidence close to the Brewster angle) around the azimuthal angle γ (see Fig. 1) while the reflected intensity was monitored by a GaAs:P diode. *In situ* exchange and the removal of samples enabled a quasi-simultaneous polarization analysis of the incident and reflected beam. The samples were highly-oriented pyrolytic graphite and amorphous carbon. The latter sample was a commercial "Univeks carbon wafer" obtained from UNITIKA LTD, Osaka 541-8566, Japan.

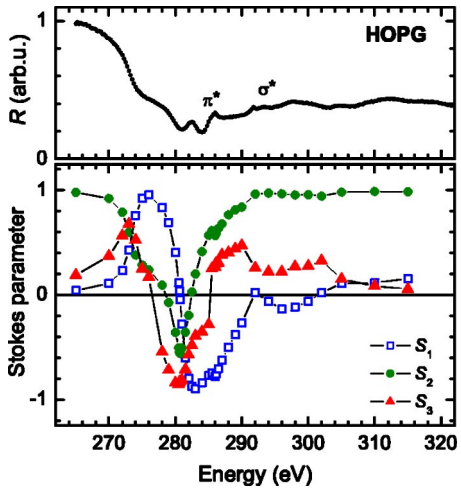

FIG. 2. (Color online) Top panel: the measured reflectance R of graphite. The incident light is linearly polarized light with $\theta_i = 87.5°$ and $\alpha = 45°$ (see Fig. 1), i.e., the Stokes parameters of the incoming light are $S_1 = 0$, $S_2 = 1$, $S_3 = 0$. Bottom panel: the Stokes parameters S_1, S_2, and S_3 of the reflected light measured by polarization analysis. The x-ray birefringence indicated by the dramatic change of the Stokes parameters is most pronounced in the range between 270 eV and 290 eV.

III. RESULTS AND DISCUSSION

The optical anisotropy of graphite is well known to result from the layered structure of hexagonal graphite, in which the pronounced crystalline anisotropy gives rise to the known structural and electronic properties.[33–36] The carbon atoms in the hexagonal basal plane are strongly bound by covalent (σ) bonds, while the bonds between adjacent planes are of the weak van der Waals type. The interlayer nearest neighbor distance (3.35 Å) is consequently much larger than the intralayer nearest neighbor distance (1.42 Å). These bonding properties are ascribed to the formation of sp^2 hybrids. In the graphene plane, the p_x and p_y orbitals result in trigonally directed sp^2 hybrids, forming σ bonds while electrons in the p_z valence orbitals perpendicular to the σ bonding plane are forming weak π bonds. Graphite is thus a typical uniaxial crystal, having the optical axis perpendicular to the sp^2 plane, which usually forms parallel to the surface. In contrast, diamond is an optically isotropic material due to the occurring sp^3 coordination and therefore no birefringence is expected. Also amorphous carbon possessing an unoriented local sp^2 coordination does not show a long-range crystalline order and thus birefringence is expected to be negligible. It should be noted that the x-ray natural linear birefringence is distinct from classical angular-dependent absorption measurements[33] which are also sensitive to the relative orientation of the optical axis and the linear polarization of the light. In x-ray birefringence experiments a polarization analysis of the reflected light is performed, whereas in angular-dependent absorption experiments only absorption coefficients are measured, thus yielding no information on the polarization state of light.

The reflectance spectrum of linearly polarized light across the C 1s edge of graphite is shown in the top panel of Fig. 2. This is the averaged reflectance of R_s and R_p since $\alpha = \pi/4$. The structures below 290 eV are assigned to resonant excitations, related to transitions from the C 1s level to π^* states.[33,36] Excitations to the σ^* continuum appear above 290 eV. Polarization measurements were performed at fixed photon energies across the C 1s edge by rotating the analyzer around the beam (see Fig. 1) to finally obtain the energy-dependent rotation and ellipticity spectra of the x-ray birefringence. By fitting the results to the intensity dependence of the analyzer curve $I = I_0(1 + P(S_1 \cos 2\gamma + S_2 \sin 2\gamma))$, the intensity I_0 and the Stokes parameters S_1 and S_2 were obtained (Fig. 2, bottom). The degree of circular polarization is determined from $S_3 = (1 - S_1^2 - S_2^2)^{1/2}$ assuming fully polarized incident light. The polarizing power P of the analyzer at the C 1s edge was determined independently ($P = 0.985$) before the experiment. Alternatively, we can fit in a different manner, using the expression $I = I_0(1 + PP_L \cos(2\gamma - 2\varphi))$, which provides φ directly, while ε follows from the degree of linear polarization $P_L = |\cos 2\varepsilon|$. Thus, ε can only be determined up to its sign in this way.

Dramatic changes of the Stokes parameters are visible at the C 1s edge, which are most pronounced in the range between 270 eV and 290 eV. Before the edge, at 265 eV the polarization state of the reflected light is practically unaffected. It is nearly linearly polarized with diagonal orientation of the polarization plane ($S_2 \approx 1$). As the photon energy increases the Stokes parameters change considerably. At around 276 eV the linear polarization plane is rotated by 45° yielding $S_1 \approx +1$. Around 280 eV the light changes from linear to almost circular, as indicated by $S_3 = 0.9$. At 283 eV the reflected light is again fully linearly polarized but with horizontal orientation of the polarization plane ($S_1 \approx -1$). The detailed rotation and ellipticity spectra, which follow directly from the Stokes parameters according to Eq. (5), are shown in Fig. 3. The rotation (top panel) increases with the photon energy and shows large values, reaching the maximal achievable rotations of +90° and −90° at about 280 eV in the energy range below the π^* transitions. Moving to higher energies above the π^* related transitions the rotation fades out and only small values are observed in the energy range dominated by σ^* transitions. This observation confirms the expectation that the birefringence is predominantly related to the anisotropic sp^2 coordination in graphite, in which there is a considerable anisotropy between the p_x, p_y orbitals in the hexagonal planes and the p_z orbitals perpendicular to the plane.

As a test of the above conclusions we measured the rotation angle and ellipticity of amorphous carbon. The unoriented local sp^2 coordination of amorphous carbon as well as the sp^3 coordination of diamond is expected to lead to an isotropic ordering, having a vanishing optical anisotropy and, as a consequence, a negligible birefringent rotation. Indeed, this is what we observe (Fig. 3, top panel). The rotation of amorphous carbon is smaller than that of graphite by a factor greater than 20, showing only a 4° maximum rotation. The energy dependence, however, is similar to that of graphite, i.e., restricted mainly to the range near the π^* transitions. From this observation we conclude that the small x-ray birefringence present in the data is most likely due to a fraction

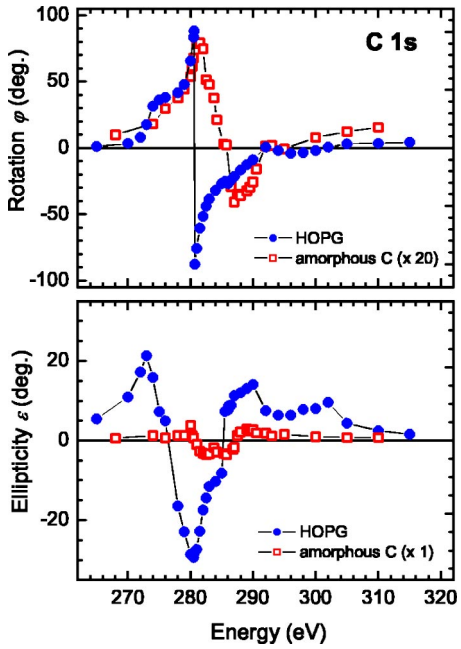

FIG. 3. (Color online) The measured x-ray birefringence of graphite and of amorphous carbon across the carbon 1*s* absorption edge, for $\theta_i = 87.5°$. Top panel: the birefringent rotation φ of the polarization plane of the reflected beam. The birefringence in reflection is large for graphite while it is small for amorphous carbon. Bottom panel: the measured birefringent ellipticity ε.

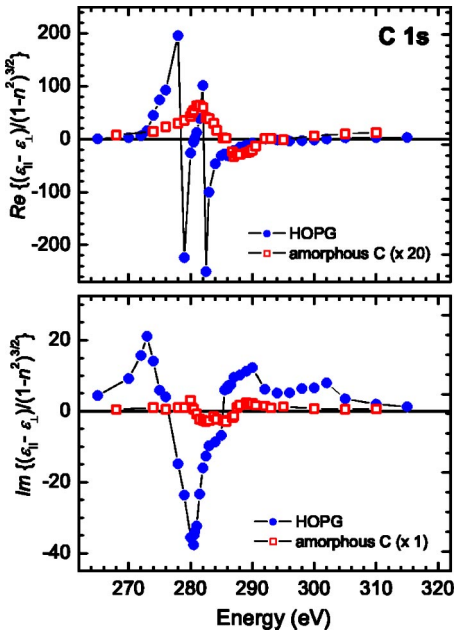

FIG. 4. (Color online) The optical anisotropy in the permittivity elements [scaled with $(1-n^2)^{3/2}$] for graphite and amorphous carbon, as determined from the x-ray birefringence measurements. Top panel: real part, bottom panel: imaginary part.

of sp^2 coordinated carbon at the surface of the sample giving rise to a small optical anisotropy. An even smaller contribution is expected to be due to the isotropic term in Eq. (4), which should not be dependent on the particular *sp* hybridization.

The ellipticity induced by the x-ray reflection from graphite is shown in the bottom panel of Fig. 3. The ellipticity reaches maximally −30° at about 280 eV. The polarization analysis in the present set-up reveals only the absolute value of ε. Therefore the sign of the values is extrapolated in accordance with the Kramers-Kronig relations.[37] From the rotation and ellipticity data we can directly compute both the real and imaginary part of the optical anisotropy given by $(\varepsilon_\parallel - \varepsilon_\perp)/(1-n^2)^{3/2}$. This quantity is shown in Fig. 4 for graphite and amorphous carbon. To obtain the optical anisotropy in the permittivity $\varepsilon_\parallel - \varepsilon_\perp$, the measured spectra must be rescaled by the refractive index *n*. However, the precise spectrum of the refractive index *n* at the edge has not been determined. Data from literature are not used since we do not want to rely on refractive indices obtained in different experiments. Note that the full complex optical anisotropy cannot be obtained experimentally from absorption spectra, which yield only the imaginary part.

To compare our data with independent predictions of the phase shift for graphite[14] we calculate the phase shift $\delta = -\arctan(S3/S2)$ from the spectra in Fig. 2. The spectral dependence of δ is understandably rather close to that of the ellipticity ε (see Fig. 3, bottom). Our experimental data agree with regard to the magnitude of the predicted maximal phase shift of up to 90°. However, the spectral shape differs significantly. The calculations of Ref. 10 show only a region above 290 eV and predict maximal effects near the σ^* transitions. In our experiment we observe a maximum shift near the π^* transitions below 290 eV. We note, however, that the calculations were carried out for $\theta_i = 83°$ while our experiments are performed at a more grazing incidence of 87.5°, which may also contribute to the discrepancy.

For a comparison with the x-ray birefringence we determined the XNLD asymmetry parameter *A* by measuring the reflectance spectra R_p and R_s [see Fig. 5(a) for graphite]. According to Eq. (6) the XNLD and S_1 should agree. This we indeed observe for graphite as well as for amorphous carbon [see Fig. 5(b)]. However, at energies near the π^* transitions the spectra for S_1 and the XNLD asymmetry differ in the case of graphite. The XNLD signal is perturbed by flourescence decay, which occurs at the absorption edge. Thereby the XNLD asymmetry is reduced, an effect which is well known from the XMLD.[12] The polarization measurement is less sensitive to fluorescence disturbances, because the analyzer is energy selective and set to select the incident light energy while the flourescence light of lower energy is suppressed. For amorphous carbon we find agreement for the XNLD *A* and S_1 [Fig. 5(b)]. Furthermore, the approximate relation $A \approx 2\varphi$ [Eq. (6)] is indeed found to be obeyed. Thus, as expected on account of the analytical relations, the x-ray natural birefringence can be accessed by different spectroscopic techniques.

One striking feature of the birefringence spectra (Figs. 2 and 3) is the appearance of large features near 276 eV and 280 eV, below the π^* transitions. These features are well understood and explained by two effects. First, the penetration depth of the incident light below the absorption edge is enlarged which leads to an increased number of graphite lay-

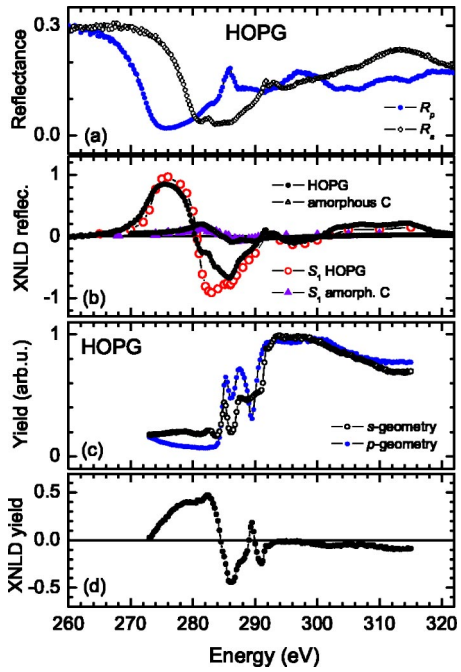

FIG. 5. (Color online) A comparison of the x-ray natural linear dichroism (XNLD) measured in reflection, the x-ray birefringence obtained from polarization analysis, and the x-ray natural linear dichroism measured in x-ray absorption, each at $\theta_i = 87.5°$. (a) The reflectance spectra R_s and R_p of graphite in *s*- or *p*-polarization geometry across the carbon 1*s* edge. (b) The measured XNLD-reflection asymmetries of graphite and of amorphous carbon, and their Stokes parameters S_1 of the reflected light (see Fig. 2). The XNLD asymmetry and the Stokes parameter S_1 agree in accordance with Eq. (6). (c) The x-ray absorption spectra of graphite recorded for the *s*- and *p*-polarization geometry, respectively. (d) The XNLD yield of graphite obtained from the spectra shown in (c).

ers contributing to the birefringence. This will be discussed in detail below. Second, the spectral dependence of the birefringence is determined by the optical constants [Eq. (4)]. Structures observed in absorption are governed by the imaginary part of the optical constant and directly resemble electronic transitions. Conversely, spectra obtained in reflection are influenced also by dispersion, i.e., by both the real and imaginary parts of the optical constant. In particular the denominator in Eq. (4) can induce additional large structures away from those resulting from direct electronic transitions if $n \approx 1$, something known to occur from x-ray magnetic reflectometry.[11,38] The influence of the optical constant on the reflection spectra is demonstrated experimentally by R_p and R_s [Fig. 5(a)], which show a strong decrease far below the C 1*s* edge. Note that the onset of the decrease for *p*-polarized light is shifted by about 6 eV to lower energies with respect to that of *s*-polarized light. This is due to the difference in the excitation energy of π^* and σ^* transitions, respectively.[33] The spectral dependence of the reflectance in turn is the result of the anisotropy in the orientation-dependent optical constants $n_\parallel \approx n_p$ and $n_\perp \approx n_s$, respectively. While *s*-polarized light excites—in the present geometry—predominantly the σ^* transitions, *p*-polarized light excites π^* transitions, with the latter excitation threshold shifted to lower energy.

To investigate further the above mentioned first point, x-ray absorption spectra were measured by collecting the total photo-electron current for both *s*- and *p*-polarized light at grazing incidence on graphite [see Fig. 5(c)]. The onsets of the σ^* transitions near 290 eV and π^* transitions around 285 eV are clearly observed. In the region 280 eV to 290 eV several spectral features have been reported previously, which were attributed to the altered local geometry and chemical environment. In particular, several C—H* structures and unsaturated C—C π^* bonds have been ascribed to these features.[33] Minor features related to π^* bonds have been related to chemical shifts at the surface or grain boundary. The corresponding XNLD absorption asymmetry parameter is plotted in Fig. 5(d). The largest asymmetry values are obtained across the π^* transitions and at the onset of σ^* transitions, similar to the results from reflectometry (Fig. 5(b)) and polarization analysis. Above the σ^* transitions the XNLD is negligible as discussed above. Note that we measure here the electron-yield XNLD in a different way compared to the frequently used method in which a difference spectrum is created from two spectra measured at normal and grazing incidence, respectively. Our method benefits from an APPLE-II type undulator where the polarization plane can be rotated.[31] This has the advantage of probing the identical sample region, i.e., with fixed penetration depth of the light, because the angle of incidence is held fixed while the polarization of the incident light is rotated.

An important difference between the x-ray absorption technique and the ellipsometric measurements lies in the probing depth. While the electron-yield spectra probe the surface-near top layer of some nm thickness, the ellipsometric spectra probe predominantly the volume of the sample. As mentioned above, the ellipsometric probing depth is directly correlated to the penetration depth of the incident light, which is inversely proportional to the absorption constant μ. This fact leads to an enhancement of the rotation angles below the π^* transitions in addition to the effect resulting from the pure optical anisotropy. With increasing absorption constant the number of graphite layers contributing to the XNLD in reflection decreases and thus the total XNLD-reflection signal is reduced. This tendency is found from Figs. 5(b) and 5(c).

The large birefringence observed in graphite has far reaching technological consequences as already suggested by theory.[14] A new avenue is opened up for the development of soft x-ray quarter-wave or half-wave plates. X-ray reflection birefringence allows to convert the polarization from linear to fully circular as well as to rotate the linear polarization plane by ±90° over a wide energy range across the C 1*s* edge. Furthermore, the polarization is tunable by rotating the graphite around the azimuth α. The largest effects are obtained for $\alpha = 45°$. For $\alpha = 0°$ and 90° the effect is "switched off." Such a device is currently not available for the C 1*s* edge.[32] Only phase shifters based on transmission multilayer optics are presently available for a fixed energy near 277 eV yielding small phase shifts of maximal 22°,[39] which are insufficient to create fully circularly polarized light. A striking advantage of our proposed x-ray quarter-wave plate is its reduced heat load sensitivity since it operates in reflection instead of transmission. This can be of interest for applica-

tions on new, high-intensity light sources, e.g., free electron lasers. In particular, in the fields of molecular physics, biology, or x-ray microscopy of living cells[40] one could benefit from these developments. Our observations are also of importance for the design of soft x-ray beamlines for circularly polarized synchrotron radiation. Here, problems could arise if the mirrors usually working under grazing incidence are contaminated with carbon that shows a strong crystalline anisotropy. For this case the degree of circular polarization of the light would significantly be reduced and linearly polarized or circularly polarized light with inverted helicity could enter the experiment at the end of the beamline. The situation would be much less serious if the mirrors are contaminated by amorphous carbon, which exhibits no crystalline anisotropy.

IV. CONCLUSIONS

We have demonstrated the existence of the x-ray natural birefringence in reflection by performing a polarization analysis of the reflected light at the C 1*s* edge of graphite. We have substantiated our claim of the observation of the x-ray birefringent rotation and ellipticity by measurements of the related Stokes parameters and of the XNLD in reflection. The natural birefringence in reflection is a much stronger effect in the soft-x-ray regime than in the visible regime due to the enhancement caused by the refractive indices in the soft-x-ray regime. Our observation emphasizes that x-ray scattering factors are to be treated as an anisotropic tensor quantity (see, e.g., Ref. 41) for crystalline materials instead of a purely atomic quantity. The technique presented here is suited to sensitively probe the electronic and corresponding structural anisotropy of any uniaxial material in the soft-x-ray range.

The large birefringent rotations and ellipticities observed in our experiment may have far reaching technological implications. On the basis of HOPG, novel optical elements like x-ray polarization modulators, quarter-wave, or even half-wave plates at the C 1*s* edge could be constructed. Such a device, based on the birefringent reflection from graphite, would allow for a tunable conversion of linearly to fully circularly polarized x rays as well as for the rotation of the polarization plane across the carbon 1*s* edge which may initiate new avenues for research employing spectroscopy at the carbon 1*s* edge, as e.g., biological investigations using polarization sensitive x-ray microscopy.

ACKNOWLEDGMENTS

The polarization analyzer was prepared by H. Grimmer, PSI-Villigen and the project was supported financially by the German Federal Ministery for Education and Science (BMBF, No. 05KS1IPB/8).

*Corresponding author: Hans-Christoph Mertins. Electronic address: mertins@fh-muenster.de

[1] See, e.g., R. M. Hornreich and S. Shtrikman, Phys. Rev. **171**, 1065 (1968).
[2] D. L. Portigal and E. Burstein, J. Phys. Chem. Solids **32**, 603 (1971).
[3] L. D. Barron, *Molecular Light Scattering and Optical Activity* (Cambridge University Press, Cambridge, 1982).
[4] D. P. Siddons, M. Hart, Y. Amemiya, and J. B. Hastings, Phys. Rev. Lett. **64**, 1967 (1990).
[5] L. Alagna, T. Prosperi, S. Turchini, J. Goulon, A. Rogalev, C. Goulon-Ginet, C. R. Natoli, R. D. Peacock, and B. Stewart, Phys. Rev. Lett. **80**, 4799 (1998).
[6] J. Goulon, A. Rogalev, F. Wilhelm, C. Goulon-Ginet, and P. Carra, Phys. Rev. Lett. **88**, 237401 (2002).
[7] S. Di Matteo and A. G. M. Jansen, Phys. Rev. B **66**, 100402(R) (2002).
[8] S. Di Matteo, Y. Joly, and C. R. Natoli, Phys. Rev. B **67**, 195105 (2003).
[9] H.-Ch. Mertins, F. Schäfers, X. Le Cann, A. Gaupp, and W. Gudat, Phys. Rev. B **61**, R874 (2000).
[10] J. B. Kortright and S. K. Kim, Phys. Rev. B **62**, 12 216 (2000).
[11] H.-Ch. Mertins, S. Valencia, D. Abramsohn, A. Gaupp, W. Gudat, and P. M. Oppeneer, Phys. Rev. B **69**, 064407 (2004).
[12] H.-Ch. Mertins, P. M. Oppeneer, J. Kunes, A. Gaupp, D. Abramsohn, and F. Schäfers, Phys. Rev. Lett. **87**, 047401 (2001).
[13] J. Humlicek, J. Kircher, H.-U. Habermeier, M. Cardona, Y. Fang, U. Welp, K. Vanderwoort, and D. Crabtree, Solid State Commun. **79**, 673 (1991).
[14] V. Sh. Machavariani, Phys. Rev. Lett. **80**, 1541 (1998).
[15] E. Filatova, A. Stepanov, C. Blessing, J. Friedrich, R. Barchewitz, J.-M. André, F. Le Guern, and P. Troussel, J. Phys.: Condens. Matter **7**, 2731 (1995).
[16] K. Harigaya, J. Phys.: Condens. Matter **13**, 1295 (2001).
[17] D. V. Khveshchenko, Phys. Rev. Lett. **87**, 246802 (2001).
[18] G. Baskaran and S. A. Jafari, Phys. Rev. Lett. **89**, 016402 (2002).
[19] T. L. Makarova, B. Sundquist, R. Höhne, P. Esquinazi, Y. Kopelevich, P. Scharff, V. A. Davydov, L. S. Kashevarova, and A. V. Rakhmanina, Nature (London) **413**, 716 (2001).
[20] P. Esquinazi, A. Setzer, R. Höhne, C. Semmelhack, Y. Kopelevich, D. Spemann, T. Butz, B. Kohlstrunk, and M. Lösche, Phys. Rev. B **66**, 024429 (2002).
[21] P. Esquinazi, D. Spemann, R. Höhne, A. Setzer, K.-H. Han, and T. Butz, Phys. Rev. Lett. **91**, 227201 (2003).
[22] A. F. Hebard, M. J. Rosseinsky, R. C. Haddon, D. W. Murphy, S. H. Glarum, T. T. M. Palstra, A. P. Ramirez, and A. R. Kortan, Nature (London) **350**, 600 (1991).
[23] P. M. Oppeneer, H.-Ch. Mertins, D. Abramsohn, A. Gaupp, W. Gudat, J. Kunes, and C. M. Schneider, Phys. Rev. B **67**, 052401 (2003).
[24] J. Kunes and P. M. Oppeneer, Phys. Rev. B **67**, 024431 (2003).
[25] D. R. Lee, S. K. Sinha, D. Haskel, Y. Choi, J. C. Lang, S. A. Stepanov, and G. Srajer, Phys. Rev. B **68**, 224409 (2003).
[26] S. S. Dhesi, G. van der Laan, E. Dudzik, and A. B. Shick, Phys. Rev. Lett. **87**, 067201 (2001).
[27] O. Zaharko, P. M. Oppeneer, H. Grimmer, M. Horisberger, H.-

Ch. Mertins, D. Abramsohn, F. Schäfers, A. Bill, and H.-B. Braun, Phys. Rev. B **66**, 134406 (2002).
[28] P. M. Oppeneer, in *Handbook of Magnetic Materials* (Elsevier, Amsterdam, 2001), Vol. 13, pp. 229–422.
[29] R. M. A. Azzam and N. M. Bashara, *Ellipsometry and Polarized Light* (North-Holland, Amsterdam, 1987).
[30] D. S. Kliger, J. W. Lewis, and C. E. Randall, *Polarized Light in Optics and Spectroscopy* (Academic Press, Boston, 1990).
[31] K. Godehusen, H.-Ch. Mertins, T. Richter, P. Zimmermann, and M. Martins, Phys. Rev. A **68**, 012711 (2003).
[32] F. Schäfers, H.-Ch. Mertins, A. Gaupp, W. Gudat, M. Mertin, I. Packe, F. Schmolla, S. Di Fonzo, G. Soullié, W. Jark, R. Walker, X. Le Cann, M. Eriksson, and R. Nyholm, Appl. Opt. **38**, 4074 (1999).
[33] J. Stöhr, *NEXAFS Spectroscopy* (Springer-Verlag, Berlin, 1992).
[34] G. Comelli, J. Stöhr, C. J. Robinson, and W. Jark, Phys. Rev. B **38**, 7511 (1988).
[35] R. Ahuja, S. Auluck, J. Trygg, J. M. Wills, O. Eriksson, and B. Johansson, Phys. Rev. B **51**, 4813 (1995).
[36] P. R. Bressler, M. Luebbe, D. R. T. Zahn, and W. Braun, J. Vac. Sci. Technol. A **15**, 2085 (1997).
[37] Kramers-Kronig type of equations can be derived for a variety of response functions; see Ref. 26.
[38] J. Kunes, P. M. Oppeneer, H.-Ch. Mertins, F. Schäfers, A. Gaupp, W. Gudat, and P. Novák, Phys. Rev. B **64**, 174417 (2001).
[39] H. Grimmer, O. Zaharko, M. Horisberger, H.-Ch. Mertins, and F. Schäfers, Surf. Rev. Lett. **9**, 481 (2002).
[40] S. Vogt, G. Schneider, A. Steuernagel, J. Lucchesi, E. Schulze, D. Rudolph, and G. Schmahl, J. Struct. Biol. **132**, 123 (2000).
[41] S. Ji, C. Song, J. Koo, K.-B. Lee, Y. J. Park, J. Y. Kim, J.-H. Park, H. J. Shin, J. S. Rhyee, B. H. Oh, and B. K. Cho, Phys. Rev. Lett. **91**, 257205 (2003).